Prototype measurement results in a 65 nm technology and TCAD simulations towards more radiation tolerant monolithic pixel sensors

C. Lemoine [a,b,*] G. Aglieri Rinella,[a] J. Baudot [b] G. Borghello,[a] F. Carnesecchi [a]
H. Hillemanns,[a] A. Kluge,[a] G. Kucharska,[a] P. V. Leitao,[a] M. Mager,[a] L. Musa,[a] F. Piro [a]
I. Sanna [a,c] W. Snoeys [a] and M. Šuljić [a]

[a]*CERN,*
 Esplanade des Particules 1, Geneva, Switzerland
[b]*IPHC, Université de Strasbourg,*
 23 Rue du Loess, Strasbourg, France
[c]*Physics department, Technische Universität München,*
 James-Franck-Straße 1, Munich, Germany

 E-mail: corentin.lemoine@cern.ch

ABSTRACT: Early measurements on monolithic pixel sensor prototypes in the TPSCo 65 nm technology indicate a different response and radiation tolerance (up to 5×10^{15} 1 MeV n_{eq} cm) for different sensor layout and process variants, illustrating the importance of layout and process in the path towards increased sensor radiation tolerance. Using these measurement results, TCAD simulations provide more insight to link the macroscopic behaviour of specific sensor variants to the details of its structure. With this insight we can propose a new variant combining the advantages of several measured variants as a path to even better radiation tolerance for the next iteration.

---

*Corresponding author.

Contents

1 Introduction

The evaluation of the TPSCo 65 nm technology in the framework of the CERN Experimental Physics Research & Development program in collaboration with the ALICE ITS3 project led to the production of sensor test structures in different process and pixel sensor layout variants [1] and their irradiation up to 1×10^{16} 1MeV n_{eq} cm^{-2}. In this context, the Analog Pixel Test Structure (APTS) [2], a monolithic sensor prototype containing 4×4 pixels each featuring an analogue output, aims at characterising the charge collection properties of the sensor. Early measurements with a ^{55}Fe source on these chips indicate that the sensor signal and its evolution with NIEL fluence are highly dependent on the process and layout variant.

This paper focuses on two process variants called split 1 and split 4. Both variants implement the same structure shown in figure 1 or in [3], with the main difference being the doping level of the deep n-type implant: split 1 is more heavily doped than split 4. Section 2 presents measurement results for the two splits before and after neutron irradiation, sections 3 and 4 analyse it with TCAD simulation and section 5 introduces a new sensor optimization.
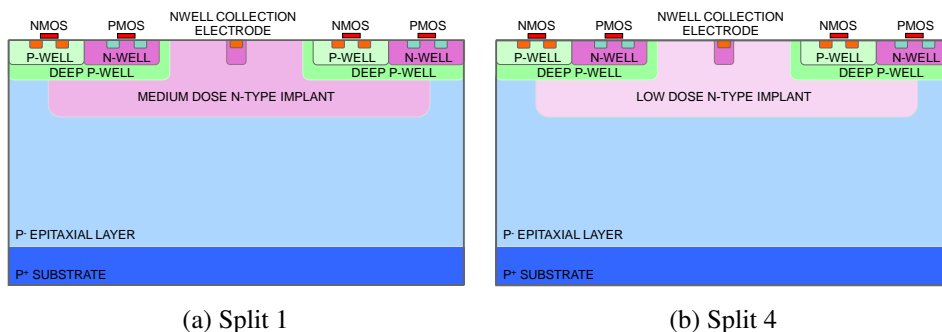

Figure 1. Cross section of the sensor for the two variants under study.

2 Measurement results

Figure 2 shows the spectrum for the two sensor variants obtained with an ^{55}Fe source before and after neutron irradiation. In this paper, the sensor substrate and pwells are always reverse biased at -4.8 V. The lower signal amplitude of the K_α peak measured in split 1 can only be explained by a higher capacitance of the sensor, coherent with the higher doping of split 1. Indeed the amplitude is inversely proportional to the total capacitance seen at the sensing node. The different splits affect mainly the sensor capacitance, but also the connecting line to the front end, and the front end itself contribute to the total capacitance. After irradiation at high fluence, the K_α peak shifts to higher amplitude for split 1, corresponding to a decrease of capacitance, still remaining higher than split 4. No such capacitance decrease is observed in the case of split 4 but, after irradiation, the charge sharing peak becomes dominant, indicating that split 4 might not be suited for use after irradiation at high fluence.[1]
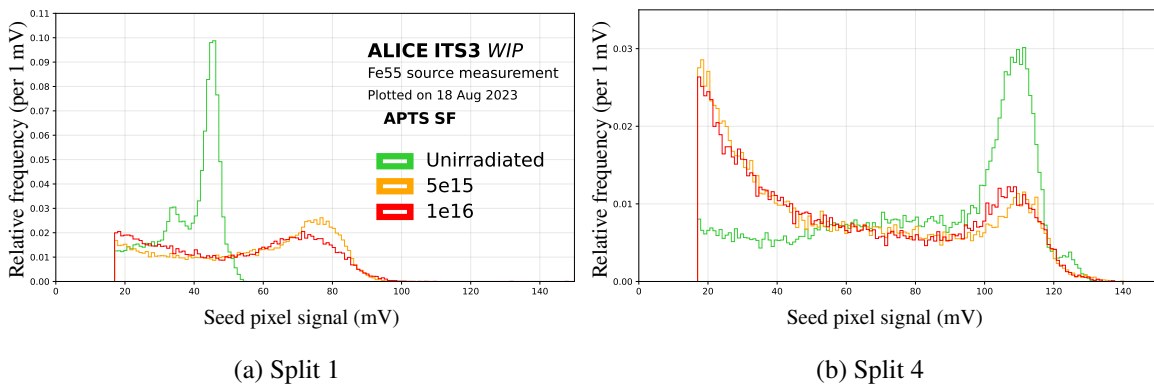

(a) Split 1   (b) Split 4

Figure 2. Measured ^{55}Fe spectra before and after neutron irradiation.

3 TCAD simulations

To better understand the measurement results, Technology Computer Aided Design (TCAD) simulations were performed. For confidentiality reasons, the 3D simulations with accurate doping profiles performed in-house will be illustrated in this paper by 2D simulation with modified doping profiles, with results matching the ones of the realistic simulations.

TCAD simulation yields a capacitance of 4.8 fF for split 1 and 1.1 fF for split 4, coherent with measurements. The difference in capacitance can be explained by an undepleted region around the collection electrode in split 1 due to the higher doping. This undepleted region can be visualized in figure 5, it is the region in red, where the weighting potential is 1.

Not only capacitance matters for the performance of the sensor, the ability to collect charges is also crucial, mostly determined by the electric field inside the sensor: its magnitude and some field lines (pointing in opposite direction of the field to describe the drift path of electrons) are plotted in figure 3. Both plots share the same scale, and a lower electric field region can be spotted at the edge between the two pixels of split 4. One can assume that this lower field will cause slower charge collection when charges are deposited at or near the pixel edge [4].

---

[1]Still to be confirmed with detection efficiency evaluation in test beam.
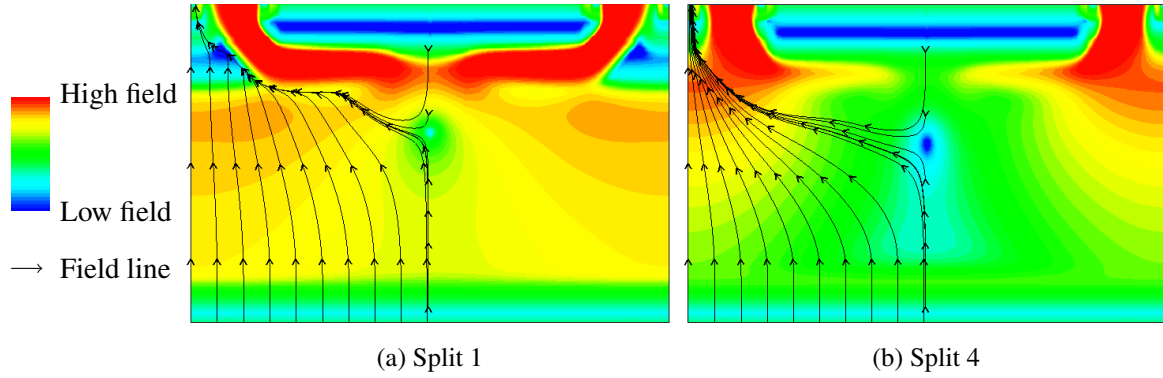
(a) Split 1   (b) Split 4

Figure 3. Simulated electric field before irradiation, centred between two pixels.

A TCAD transient simulation of a mininum ionizing particle (MIP) perpendicularly hitting the sensor, generating about 60 e/h pairs per μm, confirms this: figure 4 compares the current flowing in the collection electrode, for both splits, for a hit at the pixel center (dashed lines) and at the pixel edge (solid lines). There is a significant difference between the two variants for a hit at the pixel edge: split 1 shows a higher, shorter and less delayed pulse compared to split 4 due to the weaker field. For a hit in the pixel centre, in dashed line, the pulse amplitude is similar for both splits despite largely different electric fields. It is worth to note that the charge collection presented here (but also in figures 7 and 10) is distinct and independent of the capacitance. To obtain the voltage signal measured in the sensor one would need to integrate the pulse of figure 4 and divide it by the capacitance of the respective sensor. In addition, in the absence of trapping, both splits collect all charges from the sensitive volume after a long enough time.

To complement the information provided by the electric field in figure 3, the weighting potential is plotted for one pixel in figure 5. Due to the different undepleted region, the two variants feature a different effective collection electrode and thus a different weighting field. This knowledge allows to better understand the shape of the signal induced by a particle. As an example, in split 1 the weighting potential is non zero in the pixel edge, it means that charges deposited there start inducing signal as soon as they start moving, which is coherent with the solid line in figure 4(a). For split 4, charges need first to reach the non-constant weighting potential region before their movement starts inducing signal, it is coherent with figure 4(b).
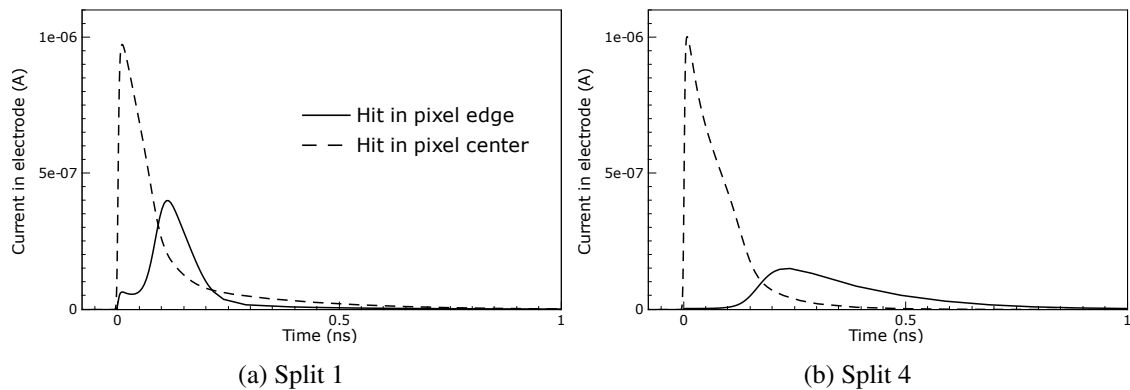

(a) Split 1   (b) Split 4

Figure 4. Simulated signal in response to a MIP crossing the unirradiated sensor.
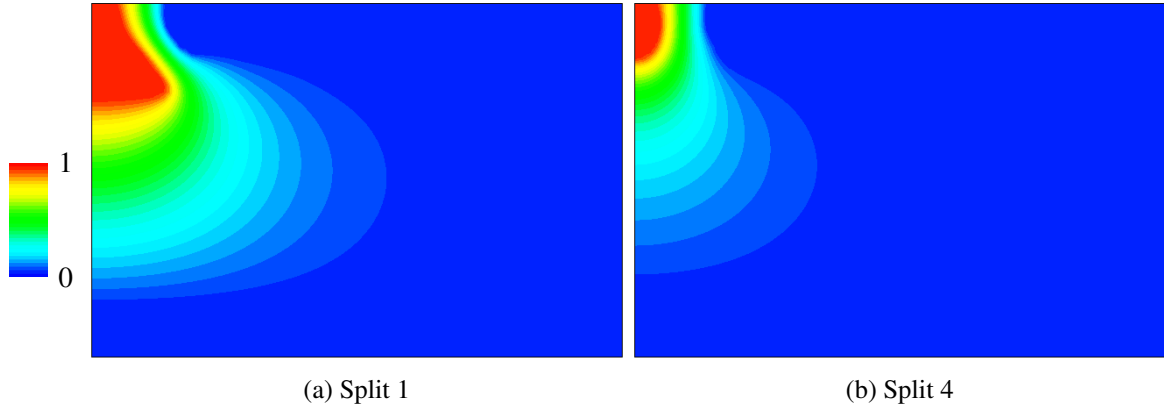
– 3 –

(a) Split 1   (b) Split 4

Figure 5. Simulated weighting potential for the left pixel before irradiation.

4 NIEL irradiation in TCAD simulations

The behaviour of irradiated sensors is simulated by introducing the so called 'new' Perugia model [5] for bulk damage in TCAD. This model introduces two acceptor and one donor trap level with a density proportional to the fluence. To avoid overfitting, no fine tuning was performed.

Simulating the capacitance of splits 1 and 4 after irradiation at 5×10^{15} 1MeV n_{eq} cm^{-2} yields 2.0 fF and 1.0 fF respectively. By comparing to the unirradiated values of 4.8 fF and 1.1 fF, it reproduces the decrease of capacitance for split 1 and the constant value for split 4.

Also the electric field changes after irradiation. As illustrated in figure 6, the low field region between pixels for split 4 extends after irradiation. Since increasing radiation fluence both increases trap density and lowers the electric field thus increasing drift time, one can expect a faster degradation of the collected charge for split 4 than split 1. This behaviour is confirmed by the transient simulation performed at different radiation fluences in figure 7. Here the current is integrated over time, thus showing the amount of collected charge.
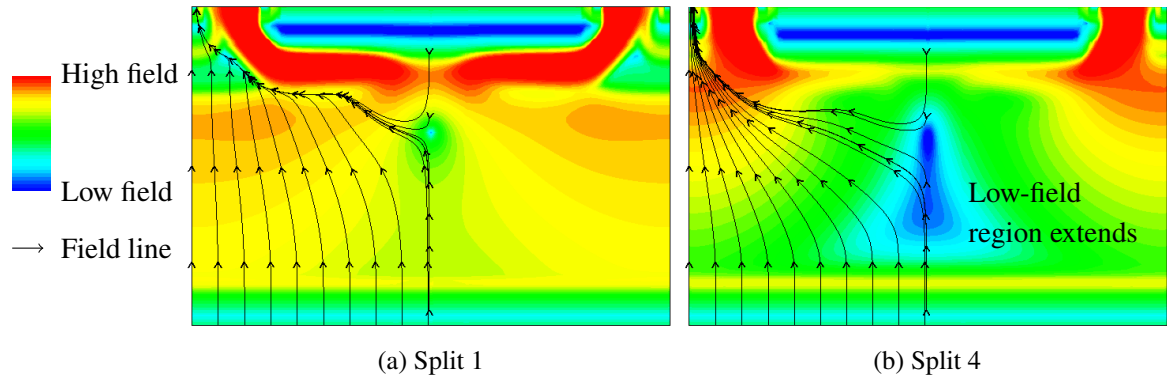

(a) Split 1   (b) Split 4

Figure 6. Simulated electric field after 5×10^{15} 1MeV n_{eq} cm^{-2}, centred between two pixels.

After irradiation, the collected charge decreases for both splits due to higher trapping, but split 4 is more affected for charge deposits near the pixel border (solid line in figure 7), not only split 1 collects more charges than split 4 after high irradiation but also collects it faster. For particle hits at the pixel centre, split 4 performs better than split 1, but this is less important as the collected charge always remains higher than the threshold value of $\approx 100\,e^-$ usually in use for such application.
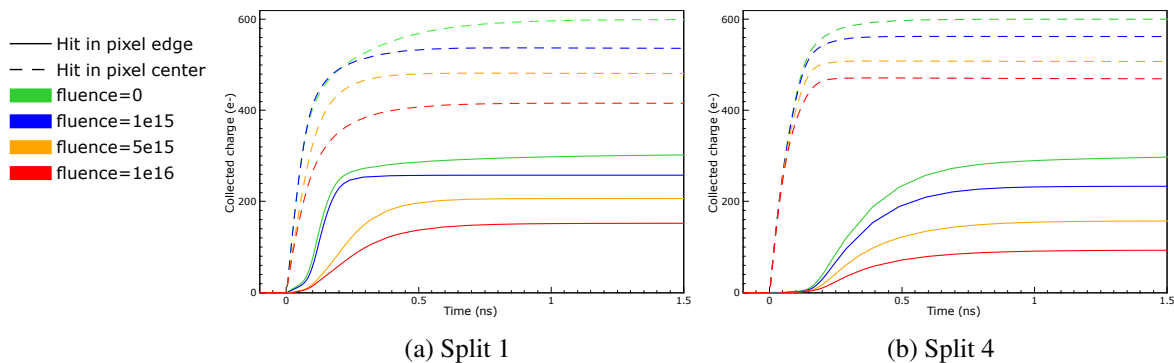
(a) Split 1   (b) Split 4

Figure 7. Integrated signal in response to a MIP crossing the sensor.

So far, two process variants were tested both in simulation and with an iron source. Some measurement observations were reproduced in simulation, giving credit to the validity of TCAD. Split 4 shows more signal amplitude than split 1 due to lower sensor capacitance, but, at high fluence, the charge collection performance of split 4 degrades more than split 1.

5 Introducing a new process variant

In order to combine the strength of both variants, we introduce a new variant named split 5, for which only simulation results are available. The process of split 5 is a mix between the ones of split 1 and split 4. As shown in figure 8, it features the high doping of split 1 below the deep pwells to achieve a good performance in the pixel corner and the low doping of split 1 below the collection electrode to maintain a low capacitance. Such design makes it possible to modify the sensor with a minimum mask change: only the deep n-type implant needs to be split in two masks.
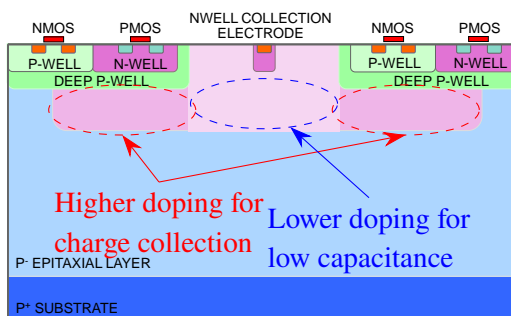

Figure 8. Cross section of the proposed new process variant (split 5).

TCAD simulations yield a capacitance for split 5 of $1.2\,\text{fF}$ before irradiation and $1.0\,\text{fF}$ after irradiation at 5×10^{15} $1\text{MeV}\,\text{n}_{eq}\,\text{cm}^{-2}$, close to the values for split 4 ($1.1\,\text{fF}$ / $1.0\,\text{fF}$). Therefore, according to simulations, split 5 inherits the low capacitance of split 4, even before irradiation.

Figure 9 shows that the electric field for split 5 at or near the pixel edge degrades slowly with irradiation compared to split 4 (figure 6). Figure 10 shows that split 5 collects approximately as much charge as split 1 after irradiation and with a fast collection, indicating split 5 also inherits the higher radiation tolerance of split 1.
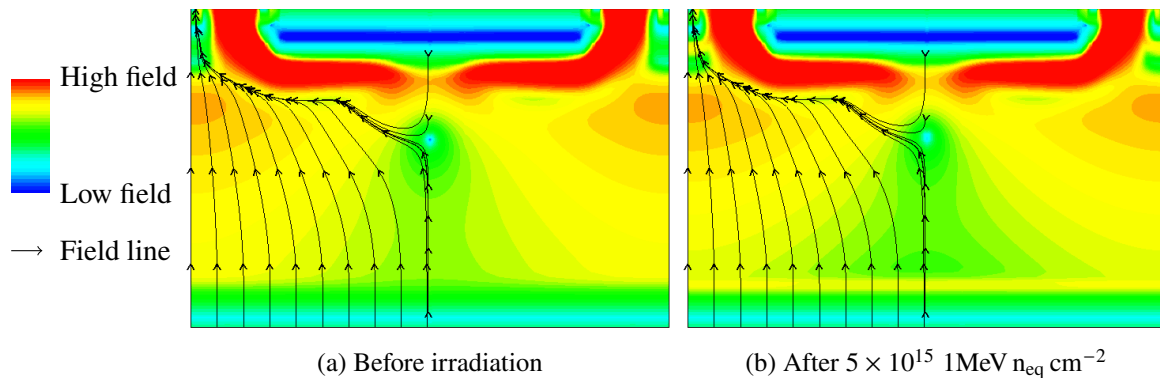
<table>
<tr><td>(a) Before irradiation</td><td>(b) After 5×10^{15} 1MeV $n_{eq}\,cm^{-2}$</td></tr>
</table>

Figure 9. Simulated electric field in the sensor of split 5, centred between two pixels.
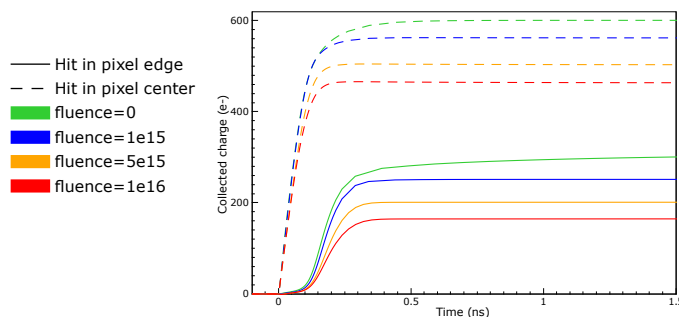

Figure 10. Integrated signal in response to a MIP crossing the sensor for split 5.

6 Conclusion

Measurement results of two sensor variants were presented, before and after irradiation. Split 4 has an excellent signal conversion capacity but a weakness in charge collection at the pixel edge. Split 1 has limited signal conversion capacity but good collection properties over the full pixel area. Applying a post-rad model in TCAD without tuning confirmed the observed trends.

With the knowledge acquired, a new optimisation was carried out with TCAD combining advantages of both variants. Performance was extrapolated for a new variant, yielding appealing results. A submission is needed to confirm those results, nonetheless this paper illustrates how TCAD can be useful in understanding measurements and providing guidance in the optimisation towards more radiation tolerant monolithic pixel sensors.

References

[1] W. Snoeys et al., *Optimization of a 65 nm CMOS imaging process for monolithic CMOS sensors for high energy physics*, *PoS* **Pixel2022** (2023) 083.

[2] W. Deng et al., *Design of an analog monolithic pixel sensor prototype in TPSCo 65 nm CMOS imaging technology*, 2023 *JINST* **18** C01065.

[3] W. Snoeys et al., *A process modification for CMOS monolithic active pixel sensors for enhanced depletion, timing performance and radiation tolerance*, *Nucl. Instrum. Meth. A* **871** (2017) 90.

[4] M. Munker et al., *Simulations of CMOS pixel sensors with a small collection electrode, improved for a faster charge collection and increased radiation tolerance*, 2019 *JINST* **14** C05013 [`arXiv:1903.10190`].

[5] F. Moscatelli et al., *Effects of Interface Donor Trap States on Isolation Properties of Detectors Operating at High-Luminosity LHC*, *IEEE Trans. Nucl. Sci.* **64** (2017) 2259.